Journal of Materials Chemistry C

ROYAL SOCIETY OF CHEMISTRY

PAPER

View Article Online
View Journal | View Issue

Cite this: J. Mater. Chem. C, 2021, 9, 4597

Influence of synthetic pathway, molecular weight and side chains on properties of indacenodithiophene-benzothiadiazole copolymers made by direct arylation polycondensation†

Desiree Adamczak,[a] Andrea Perinot,[b] Hartmut Komber,[c] Anna Illy,[a] Sandra Hultmark,[d] Bianca Passarella,[be] Wen Liang Tan,[f] Sebastian Hutsch,[gh] David Becker-Koch,[i] Charlotte Rapley,[j] Alberto D. Scaccabarozzi,[b] Martin Heeney,[j] Yana Vaynzof,[i] Frank Ortmann,[gh] Christopher R. McNeill,[f] Christian Müller,[d] Mario Caironi[b] and Michael Sommer*[a]

Received 4th January 2021,
Accepted 10th March 2021

DOI: 10.1039/d1tc00043h

rsc.li/materials-c

Atom-economic protocols for the synthesis of poly(indacenodithiophene-*alt*-benzothiadiazole) (PIDTBT) are presented in which all C–C coupling steps are achieved by direct arylation. Using two different synthetic pathways, PIDTBT copolymers with different side chains (hexylphenyl, octylphenyl, dodecyl, methyl/2-octyldodecylphenyl, 2-octyldodecylphenyl/2-octyldodecylphenyl) and molecular weight (MW) are prepared. **Route A** makes use of direct arylation polycondensation (DAP) of indacenodithiophene (IDT) and 4,7-dibromo-2,1,3-benzothiadiazole ($BTBr_2$) leading to PIDTBT in high yields, with adjustable MW and without indications for structural defects. **Route B** starts from a polyketone precursor also prepared by DAP following cyclization. While **route B** allows introduction of asymmetric side chains at the IDT unit, polymer analogous cyclization gives rise to defect formation. The absorption coefficient of PIDTBT with alkylphenyl side chains made by **route A** increases with MW. Field-effect hole mobilities around $\sim 10^{-2}$ cm^2 V^{-1} s^{-1} are molecular weight-independent, which is ascribed to a largely amorphous thin film morphology. PIDTBT with linear dodecyl side (C12) chains exhibits a bathochromic shift (20 nm), in agreement with theory, and more pronounced vibronic contributions to absorption spectra. In comparison to alkylphenyl side chains, C12 side chains allow for increased order in thin films, a weak melting endotherm and lower energetic disorder, which altogether explain substantially higher field-effect hole mobilities of $\sim 10^{-1}$ cm^2 V^{-1} s^{-1}.

Introduction

Alternating copolymers of indacenodithiophene (IDT) and benzothiadiazole (BT), PIDTBT, have shown intriguing properties as active materials in organic photovoltaics (OPVs) and organic field effect transistors (OFETs).[1–5] Due to the preserved coplanar fused aromatic ring system and thus maximized π-orbital overlap of IDT as well as low energetic disorder of PIDTBT, unique electronic

[a] Technische Universität Chemnitz, Polymerchemie, Straße der Nationen 62, 09111 Chemnitz, Germany. E-mail: michael.sommer@chemie.tu-chemnitz.de; Web: https://www.tu-chemnitz.de/chemie/polymer/
[b] Center for Nano Science and Technology @PoliMi, Istituto Italiano di Tecnologia, Via Pascoli 70/3, 20133, Milano, Italy
[c] Leibniz-Institut für Polymerforschung Dresden e.V., Hohe Straße 6, 01069 Dresden, Germany
[d] Department of Chemistry and Chemical Engineering, Chalmers University of Technology, 412 96, Gothenburg, Sweden
[e] Dipartimento di Elettronica, Informazione e Bioingegneria, Politecnico di Milano, 20133, Milan, Italy
[f] Department of Materials Science and Engineering, Monash University, Wellington Road, Clayton, Victoria 3800, Australia
[g] Department of Chemistry, Technische Universität München, 85748 Garching, Germany
[h] Center for Advancing Electronics Dresden, Technische Universität Dresden, 01062, Dresden, Germany
[i] Integrated Centre for Applied Physics and Photonic Materials and Centre for Advancing Electronics Dresden (cfaed), Technical University of Dresden, Nöthnitzer Str. 61, Dresden, 01187, Germany
[j] Department of Chemistry and Centre for Processable Electronics, Imperial College London, London W12 0BZ, UK

† Electronic supplementary information (ESI) available: experimental details, general measurements and characterization; additional NMR, SEC, IR, UV-vis, TGA and DSC data. See DOI: 10.1039/d1tc00043h

properties have been observed.[6–8] In OPV devices, PIDTBT:fullerene ($PC_{71}BM$) blends achieved power conversion efficiencies (PCE) over 6%.[9,10] Recently, small molecules based on an IDT-BT core structure were investigated as replacements for fullerene-based acceptors.[11–13] Despite their rigid backbone structure and morphologies lacking long range crystalline order,[1,14] IDT copolymers are known for their excellent charge transport properties. The combination of IDT and BT units gives rise to a rigid copolymer chain with steep torsion potential, thus favouring charge transport.[1,3] Alkyl-substituted P(IDT-*alt*-BT) copolymers exhibited low conformational disorder and field-effect mobilities up to $\mu_{sat} = 10\ cm^2\ V^{-1}\ s^{-1}$.[3,5,15] It is further noted that IDT-based materials with alkyl side chains are mostly used for transistor applications, while those with alkylphenyl side chains are designed for OPV materials. While the influence of IDT side chains has been investigated for different aliphatic ones,[2,16] the influence of alkylphenyl side chains on properties of PIDTBT copolymers is less clear.

Despite their generally appealing properties, IDT copolymers suffer from tedious reaction pathways.[17–19] State-of-the-art syntheses involve several steps of traditional transition-metal-catalyzed cross couplings based on Suzuki, Negishi or Stille reactions.[10,20] To eliminate usage of undesired toxic or unstable reagents as well as byproducts, and to shorten lengthy reaction pathways simultaneously, direct arylation (DA) as an atom-economical method is highly attractive.[21–23] Direct arylation polycondensation (DAP) is meanwhile the method of choice for naphthalene diimide copolymers[24–26] and a viable alternative for the preparation of many other donor–acceptor copolymers.[27–29] Under optimized conditions, control over molecular weight (MW), a low degree of main chain defects and high yields can be achieved. To date, few reports that report IDT copolymers *via* DAP and that yield moderate molecular weights have emerged.[30–32] Recently, we reported IDT homopolymers *via* DAP.[33]

Here, we present a comprehensive study on a series of PIDTBT made by different synthetic pathways, with varying aliphatic and alkylphenyl side chains, and different molecular weight. PIDTBT can be made by direct DAP (**route A**) as well as by polymer analogous cyclization (**route B**, Scheme 1). The latter pathway leads to structurally ill-defined products with inferior properties. PIDTBT made by **route A** with alkylphenyl side chains is molecularly defined, morphology is largely amorphous and field-effect transistor (FET) hole mobilities are independent of molecular weight. In contrast, **route A** PIDTBT with linear C12 side chains exhibits red-shifted absorption with better defined vibronic structure, increased order in thin films and lower energetic disorder. These findings explain the higher FET hole mobility of PIDTBT with C12 side chains and provide a detailed overview of how side chains influence the properties of PIDTBT.

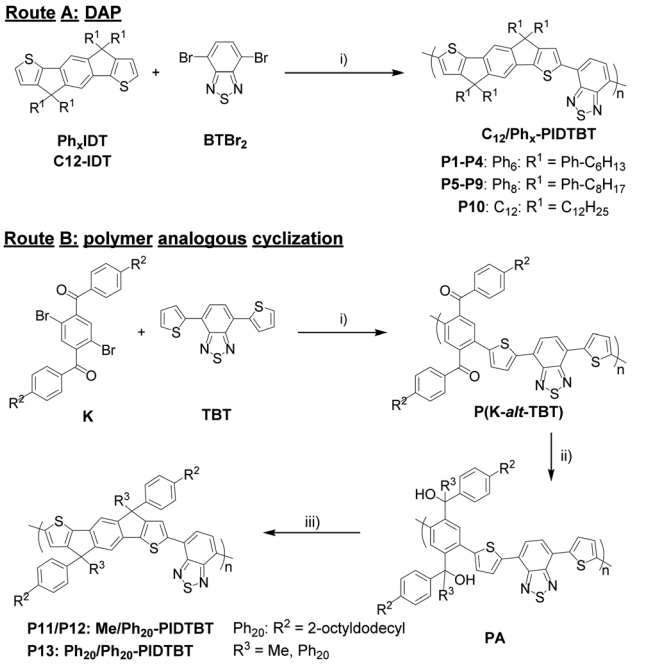

Scheme 1 Two routes for the synthesis of PIDTBT. Reaction conditions: (i) 0.05–0.25 M in mesitylene, Pd_2dba_3 (5 mol%), P(*o*-anisyl)$_3$ (20 mol%), PivOH (1 eq.), K_2CO_3 (3 eq.), 80–100 °C, 72 h; (ii) 4×10^{-3} M in toluene, R^3-Li (8 eq.), room temperature (rt), 3 h; (iii) 4×10^{-3} M in dichloromethane, $BF_3\ OEt_2$ (18 eq.), rt, 3 h.

Results and discussion

Synthesis and characterization.

The synthetic routes towards PIDTBT are shown in Scheme 1. All C–C couplings, including monomer synthesis of Ph$_x$IDT, were achieved *via* direct arylation. The optimization of IDT monomer synthesis was investigated previously.[33] Monomer K was prepared according to previous reports.[17,33,34] Copolymerization of Ph$_6$IDT with 4,7-dibromo-2,1,3-benzothiadiazole (BTBr$_2$) *via* DAP yielded Ph$_6$-PIDTBT copolymers with MWs up to $M_{n,SEC}$ = 38 kg mol^{-1}. Optimization of MW was carried out considering effects of solvent, temperature, catalyst loading and monomer concentration (Table 1, entries **P1–P9**). Lowering the reaction temperature led to an increase in MW. Regarding monomer concentration, an optimum was found for 0.1 M.

Monomer concentrations smaller than 0.1 M resulted in lower MWs due to slower build up of chain length and consequently a larger impact of termination reactions (Table 1, **P2**). Concentrations larger than 0.1 M led to early gelation of the reaction mixture (Table 1, **P4**). The use of a different solvent such as chlorobenzene to enhance solubility of the formed polymer chains enabled reactions at higher monomer concentrations and lower catalyst loadings, but did not generate higher MW (see ESI,† Table S1, entries S3–5). To increase MW further, Ph$_8$IDT was used in **route A**. However, despite the better solubility of the monomer higher MWs of the corresponding copolymers were not achieved, eventually due to a lower monomer purity as a result of more difficult purification. To change MW, a reduction of catalyst loading (Table 1, **P9**) and variation of reaction temperature (Table 1, **P1**/**P3**) can be used. For **route A**, however, adjustment of MW is best achieved by using optimized conditions of entry **P1** following slightly changed stoichiometry (Table 1, **P6**). The synthesis of C12-PIDTBT *via* DAP proceeded smoothly to give **P10** with $M_{n,SEC}$ = 32 kg mol^{-1}. In comparison to **P1** with Ph$_6$ side

Table 1 Reaction conditions for syntheses of PIDTBT made *via* **route A** and **route B**

	entry	R^1	R^2/R^3	Solvent	[M]/M	T/°C	Cat/P-ligand mol%	M_n/M_w[a] kg mol^{-1}	$Đ$[a]	Yield[b]/%
Route A	**P1**[c]	Ph_6	—	Mesitylene	0.1	80	5/20	38/130	3.4	92
	P2	Ph_6	—	Mesitylene	0.05	100	5/20	15/32	2.2	87
	P3[c]	Ph_6	—	Mesitylene	0.1	100	5/20	18/39	2.1	84
	P4[c]	Ph_6	—	Mesitylene	0.25	100	5/20	12/33	2.7	87
	P5	Ph_8	—	Mesitylene	0.1	80	5/20	28/62	2.2	79
	P6[d]	Ph_8	—	Mesitylene	0.1	80	5/20	17/38	2.2	75
	P7	Ph_8	—	Mesitylene	0.1	90	5/20	11/18	1.6	62
	P8	Ph_8	—	Mesitylene	0.1	100	5/20	21/48	2.3	95
	P9	Ph_8	—	Mesitylene	0.1	100	1/5	18/31	1.7	69
	P10	$C_{12}H_{25}$	—	Mesitylene	0.1	80	5/20	32/55	1.7	74
Route B	**P(K-*alt*-TBT)**	—	Ph_{20}	Mesitylene	0.25	90	5/20	11/15	1.4	75
	P11[e]	—	Me/Ph_{20}					21/6.6 × 10^8[f]	3 × 10^4[f]	5
	P12	—	Me/Ph_{20}					17/1.45 × 10^7[f]	833[f]	5
	P13	—	Ph_{20}/Ph_{20}					18/88	4.9	73

[a] From SEC in chloroform with PS calibration. [b] Isolated yield after Soxhlet extraction with acetone, ethyl acetate and chloroform. [c] Gelation after 24 hours. [d] A slight excess of $BTBr_2$ of 5 mol% was used. [e] Without phenyl termination. [f] Bimodal SEC curves with very large M_w and $Đ$ values likely caused by chain-chain coupling as well as aggregation whenever Me/Ph_{20} side chain patterns were used.

chains, the reaction mixture containing **P10** did not gelate during polymerization. To gain insight into details of the molecular structure of PIDTBT, NMR spectroscopy was used with assignments aided by model compounds. The ^{1}H and ^{13}C NMR spectra of the PIDTBT copolymers did not show obvious evidence for defects (Fig. S1–S4, ESI†). However, it should be noted that defects such as homocouplings[35] are generally challenging to detect for IDT copolymers as a result of significant signal broadening and overlap with backbone signals.[33] Because of the low intensity of end group signals, a comparison with spectra of appropriate model compounds is an efficient method to assign these signals in NMR spectra of copolymers (Fig. 1).[24,25] The Ph_6IDT monomer represents the IDT-H end group, and the two IDT-based model compounds **1** (Br-BTIDTBT-Br) and **2** (H-BTIDTBT-H) were synthesized to mimic BT-Br and BT-H end groups, respectively (for details see ESI†). The aromatic region of the ^{1}H NMR spectra of **P8** and **P6** are depicted in Fig. 1a and d, respectively. Comparison with the monomer Ph_6IDT (Fig. 1b and Fig. S5, ESI†) and model **2** (Fig. 1c and Fig. S7, ESI†) revealed IDT-H and BT-H termination for **P8**. The BT-Br end group (model **1**, Fig. 1e and Fig. S6, ESI†) was not detected. However, BT-Br end groups are contained exclusively in the second copolymer (**P6**), for which a slight excess of $BTBr_2$ was used. A further difference between **P8** and **P6** is reaction temperature. We assume that the lower temperature used for **P6** (80 °C) contributes to the presence of BT-Br end groups by lowering the probability for dehalogenation.

Route B entails the preparation of PIDTBT copolymers *via* DAP followed by polymer analogous cyclization (Scheme 1, **route B**).[33] Here, MW is generally strongly limited by solubility of the polyketone precursor **P(K-*alt*-TBT)**. Even long, branched side chains such as R = 2-octyldodecyl only led to moderate MW of $M_{n,SEC}$ = 11 kg mol^{-1}. The progress of the polymer analogous reactions was monitored by UV-vis and IR spectroscopy (Fig. S10 and S11, ESI†). Additional signals in the NMR spectra (Fig. S12 and S13, ESI†) and very broad and bimodal MW distributions of **P11–P13** (Fig. S14, ESI†) suggested significant structural defects of unclear nature. Efforts were made to gain further insight. To eliminate possible side reactions associated with thiophene-based end groups during the post-polymerization sequence, **P(K-*alt*-TBT)** was terminated with bromobenzene.[33] Phenyl termination of **P(K-*alt*-TBT)** reduced the very large dispersity of the corresponding PIDTBT from 3 × 10^4 to 833 (compare entries **P11** and **P12** without and with phenyl termination, respectively). Considering that dispersity of **P13** with Ph_{20}/Ph_{20} side chains is ~5 and thus comparably large, yet lower compared to **P11** and **P12**, we conclude that **P11** and **P12** with Me/Ph_{20} side chains likely show a combination of chain-chain coupling and additional aggregation.

These results from NMR spectroscopy and SEC clearly indicated significant defects of unclear nature that are unlikely to be moved entirely. Additionally, UV-vis spectra of PIDTBT made *via* **route B** were much different (Fig. 2c and d), and FET hole mobilities were much reduced (see Table 3 and further discussion below) compared to **route A**.

Obviously, **route A** is the method of choice to make well-defined PIDTBT *via* DAP, and PIDTBT made by **route B** was only further used and mentioned where helpful for a comprehensive discussion. What remains open at this point is the investigation of homocouplings in PIDTBT made by **route A**, which cannot be ruled out entirely based on the herein performed NMR spectroscopic investigations. Even with the homopolymer PIDT as model compound for IDT CH/CH homocoupling being available, the broad signals did not allow for conclusive statements here. Obtaining direct NMR spectroscopic evidence for homocouplings in PIDTBT is therefore very challenging. However, optical data (*vide infra*) suggested well-defined PIDTBT from **route A** to be formed, which is indirect evidence for the absence of such main chain structural defects.

Selected copolymers were further investigated by UV-vis and photoluminescence (PL) spectroscopy, cyclic voltammetry (CV), density functional theory (DFT) calculations, thermogravimetry (TGA), differential scanning calorimetry (DSC), fast scanning calorimetry (FSC), field-effect mobility measurements, grazing incidence X-ray scattering (GIWAXS) and photothermal deflection spectroscopy (PDS). Important

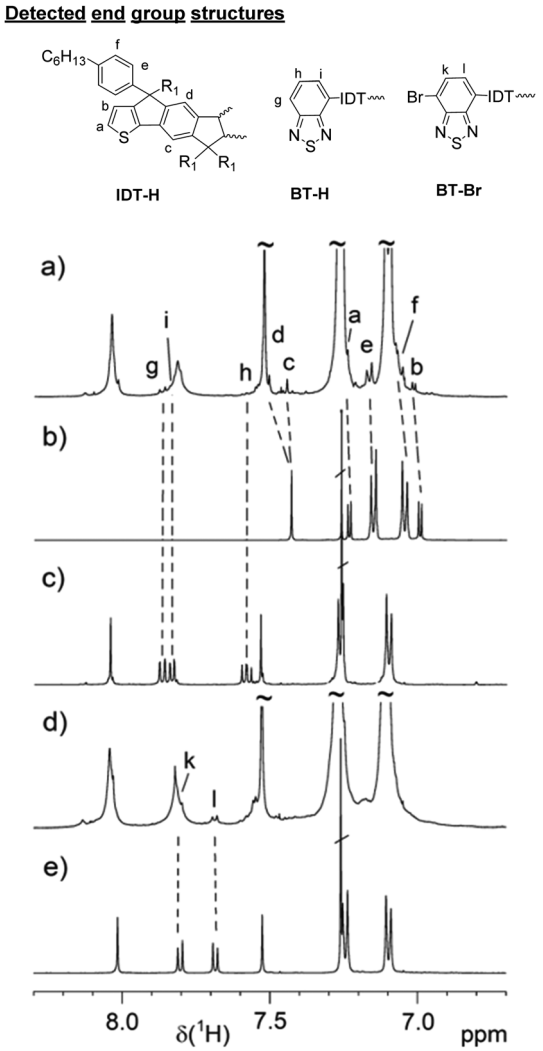

Fig. 1 ^{1}H NMR spectrum (region) of IDT- and H-BT-terminated PIDTBT (a) (**P8**) compared to the spectra of Ph_6IDT monomer (b) and H-BT model compound **2** (c). The spectrum of a Br-BT-terminated PIDTBT (d) (**P6**) is compared with the spectrum of Br-BT model compound **1** (e). R^1 = Ph_6. Solvent: $CDCl_3$.

results are compiled in Table 2 and further discussed in detail in what follows.

Optical properties

The dependence of MW of PIDTBT with Ph_8 side chains made by **route A** on UV-vis and PL spectra is shown in Fig. 2a and b. With increasing MW a slight bathochromic shift of the absorption maximum and an increase of the molar extinction coefficient $\varepsilon_{abs,max}$ can be observed. This effect can be attributed to an increasing contribution of the vibronic band at longer wavelength, which in turn may be caused by increasing chain length.[36] Notably, the similarity of the spectra in Fig. 2a including a sharp onset at large wavelength is indicative for structurally well-defined copolymers, and thus a robust synthetic DAP protocol. Intensity of PL in solution correlates similarly with MW as found for the molar extinction coefficient. Emission maxima around $\lambda_{em,max}$ = 696 nm

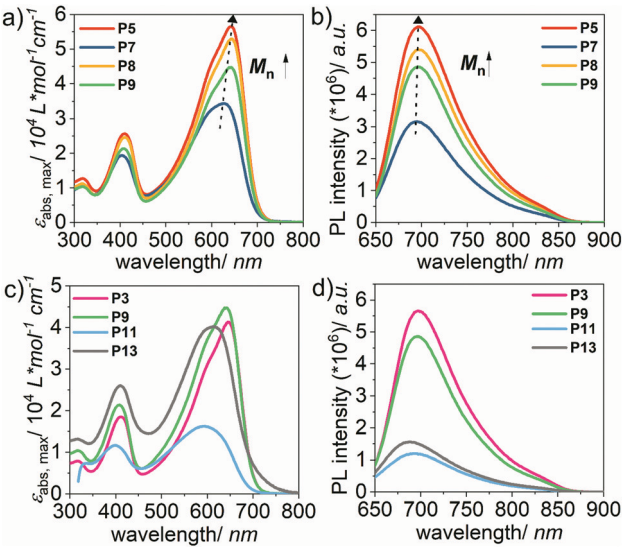

Fig. 2 UV-vis and PL spectra of PIDTBT of different MW (a and b) and of PIDTBT with different side chains (c and d) in chloroform solution. (**P5–P9**: R^1 = Ph_8, **P3**: R^1 = Ph_6, **P11**: Me/Ph_{20}; **P13**: Ph_{20}/Ph_{20}).

are weakly dependent on MW. These almost constant maxima thus result in decreased Stokes shifts for increasing MW (**P5:** $\Delta\lambda$ = 52 nm; **P7** = $\Delta\lambda$ = 68 nm). Fig. 2c and d illustrates the influence of the synthetic method and IDT side chain pattern on absorption. Small differences between the molar extinction coefficients and intensities of emission maxima of **P3** (**route A**, R = Ph_6) and **P9** (**route A**, R = Ph_8) likely arise from slightly different molar masses of the repeat unit and MWs. The UV-vis spectra of **P11** and **P13** made *via* **route B** are significantly different. The hypsochromically shifted absorption maxima as well as the up to three times smaller molar extinction coefficients suggest disruptions of the π-system due to defects produced during the cyclization step. The emission spectra display the same trends of decreased molar extinction coefficients and hypsochromically shifted spectra thus corroborating this argumentation (Fig. 2d).

The effect of aromatic *versus* aliphatic side chains on absorption is displayed in Fig. 3. Despite the slightly lower molecular weight of **P10** (R = $C_{12}H_{25}$) compared to **P1** (R = Ph_6), the absorption spectrum shows a bathochromic shift of 20 nm with the molar extinction coefficient at maximum wavelength being retained (Fig. 3a). Further differences are a smaller contribution of the vibronic shoulder around 600 nm for **P10**. The film spectrum of **P1** shows a small shift of the absorption maximum ($\Delta\lambda$ = 8 nm), suggesting little conformational changes of the chain upon solidification. The thin film absorption spectrum of **P10** displays a shift of $\Delta\lambda$ = 12 nm and additionally develops a pronounced shoulder around 630 nm indicative for increased order (Fig. 3b).

The redshifted absorption spectrum of **P10** results in a reduced optical band gap E_g compared to **P1** (E_g(**P10**) = 1.69 eV; E_g(**P1**) = 1.73 eV). The difference of the optical band gap is reflected in the HOMO/LUMO energy levels of **P1** and **P10**. Determination of the energy levels were carried out by cyclic voltammetry (Fig. S15, ESI†). The electrochemical analyses

Table 2 Optical and thermal properties of selected PIDTBT copolymers

	Entry	R^1	R^2/R^3	M_n/M_w[a]/kg mol^{-1}	$\lambda_{abs,max}$ (sol)[b]/nm	$\lambda_{em,max}$ (sol)[b]/nm	$\lambda_{abs,max}$ (film)[c]/nm	$\varepsilon_{abs,max}$[c]/10^3 L mol^{-1} cm^{-1}	T_d[cd]/°C
Route A	**P1**	Ph_6	—	38/138	*643*/410	698	*651*/416	57	—
	P3	Ph_6	—	18/39	*645*/411	697	—	41	449
	P5	Ph_8	—	28/62	*644*/410	696	*651*/414	57	427
	P7	Ph_8	—	11/18	*627*/403	695	—	34	—
	P8	Ph_8	—	21/48	*645*/411	696	—	53	—
	P9	Ph_8	—	18/31	*643*/408	696	—	45	—
	P10	$C_{12}H_{25}$	—	32/55	*664*/415	715	*682*/418	56	408
Route B	**P11**[e]	—	Me/Ph_{20}	21/6.6 × 10^8[f]	*595*/394	693	—	16	—
	P12	—	Me/Ph_{20}	17/1.45 × 10^7[f]	*596*/411	695	—	—	—
	P13	—	Ph_{20}/Ph_{20}	18/88	*615*/410	688	—	40	371

[a] From SEC in chloroform with PS calibration. [b] Measured in chloroform at room temperature. Maxima with the highest intensity in italic. [c] Measurements were carried out on selected samples. [d] Degradation temperature at 5% weight loss. [e] Without phenyl termination. [f] Bimodal SEC curves, large M_w and $Đ$ values likely caused by chain-chain coupling as well as aggregation whenever Me/Ph_{20} side chain patterns were used.

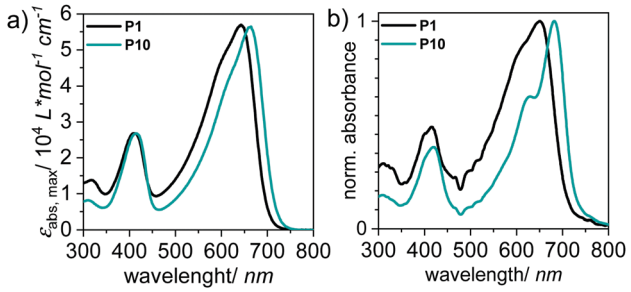

Fig. 3 Comparison of UV-vis spectra in chloroform solution (a) and film (b) of PIDTBT with aromatic (**P1**) and aliphatic (**P10**) side chain pattern *via* DAP. Films were spin coated (1000 rpm, 60 s) from *o*-DCB solutions (10 mg mL^{-1}).

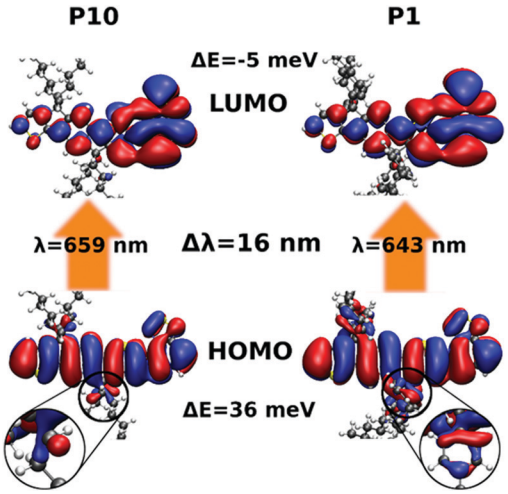

Fig. 4 Frontier orbitals and excitation energies of **P10** (left) and **P1** (right). The LUMOs (top) primarily localise at the BT units. Energy differences ΔE are based on Kohn–Sham orbital energies. The HOMOs (bottom) delocalise over the full backbone and the side chains (inset). The wavelengths λ of the low-energy excitations of **P10** and **P1** obtained from TD-DFT differ by about $\Delta\lambda$ = 16 nm (centre).

reveal a slightly higher lying HOMO energy level of **P10**. In film as well as in solution, the energy of the HOMO levels differ by ΔHOMO(film) = 50 meV and ΔHOMO(solution) = 30 meV, respectively. However, while the nature of the side chains influences the HOMO energy levels of PIDTBT, the LUMO energy level remains largely unaffected (ΔLUMO(film) = 0 meV; ΔLUMO(solution) = −1 meV). The electrochemical properties are summarized in Table S2 (see ESI†).

DFT calculations

To study the reason for the observed shift between the absorption spectra of **P1** and **P10** (ref. Fig. 3), density functional theory (DFT) calculations were performed. First, the structure and energy of the orbitals involved in the optical excitation, which are the highest occupied molecular orbital (HOMO) and the lowest unoccupied molecular orbital (LUMO), were analysed. The orbitals were calculated with DFT in Gaussian 16[37] for a single repeat unit and the complete side chains. More details to the calculations can be found in the methods section (see ESI†). The resulting orbitals and corresponding Kohn–Sham energies are presented in Fig. 4. The LUMOs are shown in the top of Fig. 4.

LUMOs primarily localise at the BT units, while the IDT units receive much less orbital weight and the side chains essentially none. As a result, the different side chains of **P1** and **P10** have a minor impact on the orbital energy of the LUMO and the Kohn–Sham energies differ by only $E^{LUMO}_{P10} - E^{LUMO}_{P1} = -5$ meV. In contrast, the HOMOs delocalise over the full backbone (bottom of Fig. 4) and expand over the alkyl chain of **P10** and phenyl group of **P1**, as shown in the insets of Fig. 4. Therefore, the side chains do affect the HOMO energies and the resulting Kohn–Sham energies differ by $E^{HOMO}_{P10} - E^{HOMO}_{P1} =$ 36 meV. As a result, the HOMO of **P10** is shifted to higher energies, while the LUMO is nearly unaffected. This decreases the single-particle gap and causes a redshift in the excitation energy. To analyse this in more detail, the first excitation energy of each structure is calculated with time-dependent DFT (TD-DFT) for an enlarged polymer backbone in solution for which we use a polymer model of three repeat units. To make the calculations computational feasible, the side chains are cut-off after the first alkyl segment, since the frontier orbitals do not significantly delocalise beyond these as shown in Fig. 4. The chloroform solution used in the experiment is modelled by the

polarizable continuum model as implemented in Gaussian 16.[37] More details on the simulation parameters can be found in the methods section (see ESI†). The TD-DFT simulations yield excitation energies of $\lambda_{\mathbf{P10}}$ = 2.329 eV (532 nm) and $\lambda_{\mathbf{P1}}$ = 2.376 eV (522 nm). However, the excitation energies calculated with TD-DFT usually show a systematic overestimation in the range of $\Delta\lambda^{\text{TD-DFT}}$ = 300–600 meV.[38,39] Here, we apply a shift of $\Delta\lambda^{\text{sim-exp}}$ = 448 meV that yields corrected excitation energies of $\lambda_{\mathbf{P10}}$ = 1.882 eV (659 nm) and $\lambda_{\mathbf{P1}}$ = 1.928 eV (643 nm), which are shown in the centre of Fig. 4. More important than the absolute position of the excitation energy, the TD-DFT simulations reveal a redshift of the excitation energy of **P10** by $\Delta\lambda^{\text{sim}}$ = 16 nm similar to the experimental observation of $\Delta\lambda^{\text{exp}}$ = 20 nm. We therefore find that the deeper and slightly more delocalized HOMO on the alkylphenyl side chains causes the observed shift. Conformation and coplanarity of the IDT is not affected by the different side chains.

Thermal properties

All polymers possess good thermal stability with degradation temperatures (5% weight loss) T_d between 370–450 °C (Table 2 and Fig. S16, ESI†). DSC second heating thermograms reveal a shallow exotherm around 90 °C (Fig. S17, ESI†), which we explain with reorganization at temperatures exceeding the glass transition temperature T_g. We note that all investigated copolymers show similar DSC traces and appear to undergo such a process in a similar temperature range, as expected for polymers with an $M_n > 10$ kg mol^{-1} for which the T_g becomes less dependent on chain length.[40] Only for **P10** with C12 side chains, a T_g of 96 °C can be determined (Fig. S17 and S18, ESI†).[41] **P10** also shows two weak transitions that are ascribed to melting (T_m = 213 °C, ΔH_m = 1.5 J g^{-1}) and crystallization (T_c = 168 °C, ΔH_c = 3.7 J g^{-1}). The weak crystallinity of **P10** is in accordance to the observations of vibronic structure seen in thin film UV-vis spectra and indicates improved intermolecular packing enabled by the more flexible aliphatic side chains compared to Ph_6-substituted PIDTBT, for which conventional DSC thermograms did not show signs of crystallization.

Due to the difficulty for all polymers to extract T_g values from conventional DSC, we additionally carried out physical ageing experiments to investigate T_g values in more detail. We chose to focus on **P13** because we expected this material to display a high degree of disorder, and hence a prominent T_g, due to the presence of main chain defects (*cf.* discussion above). The same type of experiment was inconclusive for samples made *via* **route A** (not shown). We used fast scanning calorimetry (FSC) to anneal **P13** for 30 min at T_{anneal} ranging from 30 to 140 °C, followed by rapid heating at 4000 K s^{-1} from −50 to 300 °C (Fig. 5a), which follows a protocol that has been used for other conjugated polymers.[42,43] A distinct endothermic overshoot can be discerned for each T_{anneal} with a clear minimum in enthalpy ΔH at T_{anneal} = 80 °C (Fig. 5b). We identify two temperature regimes below and above 80 °C, which we assign to enthalpy relaxation of the mobile amorphous fraction (MAF) and rigid amorphous fraction (RAF), respectively. We extrapolate an upper limit of the T_g of 88 °C, which is in agreement with the exotherms observed with conventional DSC (Fig. S17, ESI†). The same type of experiment was performed on C12-PIDTBT **P10** to investigate the influence of the side chains on the relaxation kinetics of the polymer backbone and hence the T_g of the polymer.[40] FSC measurements reveal a slightly higher T_g of 98 °C (Fig. 5c). The rather small difference in T_g between **P10** and **P13** is remarkable considering the very different nature of side chains in the two polymers. The larger side chains of **P13** (52 carbons) compared to **P10** (24 carbons) are expected to decrease T_g of the former,[44] but this effect may be partially compensated by the phenyl rings that are part of the side chains of Ph_{20}, which cause an increase at a constant number of carbons.[40,45]

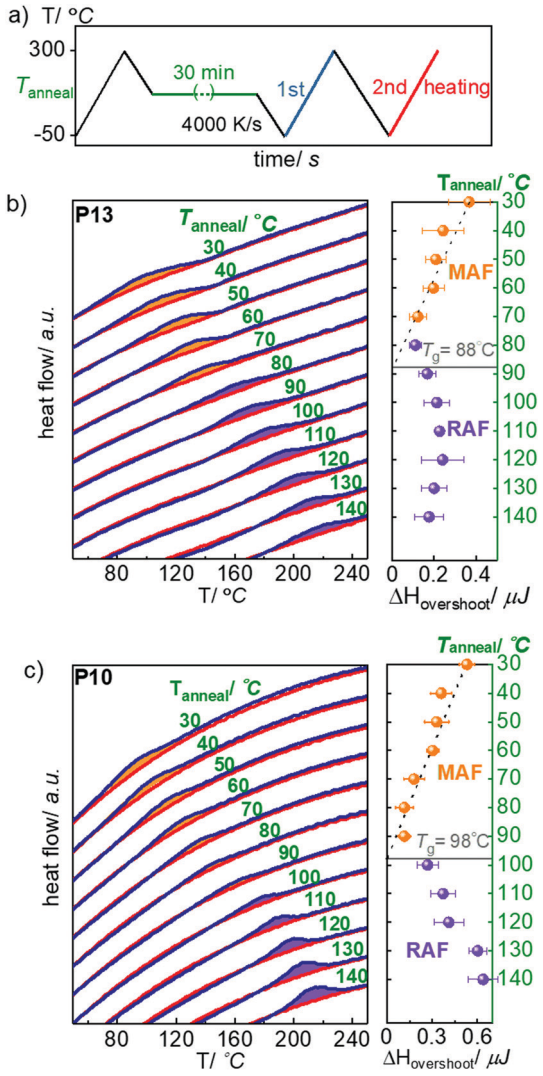

Fig. 5 (a) Protocol used for FSC measurements comprising a heating scan after physical ageing for 30 min at annealing temperature T_{anneal} (blue) and a second reference heating scan from -50 to 300 °C (red); FSC heating thermograms of (b) **P13** and (c) **P10**, after ageing (blue) and corresponding reference scans (red) as well as the enthalpy of the endothermic overshoot ΔH as a function of T_{anneal}; the dashed line represents the extrapolation of the upper limit of the T_g.

Electrical properties

The charge transport properties of the polymers thin films were investigated with field-effect transistors, using a standard top-gate bottom-contact configuration characterized by a channel length of 20 μm (Fig. S19–S22, ESI†). The extracted values for the apparent charge mobility in the saturation regime ($V_d = V_g = -60$ V) are summarized in Table 3.

The hole mobilities of the polymers *via* **route A** are in the range of μ_{sat} = 0.02–0.04 cm^2 V^{-1} s^{-1}, in line with values reported for polymer analogues made by Stille coupling.[9,10] Reducing the channel length to 5 μm leads to a slight improvement of mobility in a similar manner for all investigated copolymers, up to μ_{sat} = 0.05 cm^2 V^{-1} s^{-1}. We tentatively attribute the channel length dependence to lateral-field enhancement of charge transport and/or injection.[46] In general, the measured values of PIDTBT with alkylphenyl side chains are one order of magnitude lower than C12-substituted PIDTBT **P10** (Fig. S21, ESI†). This effect may be caused by the steric hindrance of the rigid phenyl rings that reduce intermolecular stacking of backbones and thus a contribution from interchain transport.

Unlike alkyl-substituted PIDTBT where longer alkyl chains as well as higher MW lead to improved μ_{sat} by up to one order of magnitude (R = octyl, μ_{sat} = 0.15 cm^2 V^{-1} s^{-1}; R = hexyldecyl, μ_{sat} = 1.2 cm^2 V^{-1} s^{-1})[2], alkylphenyl-substituted PIDTBT neither exhibits a MW nor a side chain length dependence (Fig. S19 and S20, ESI†). PIDTBT **P11-P13** made by **route B** exhibits decreased transport performance with mobilities smaller by two to three orders of magnitude that obviously result from defective backbones (Fig. S22, ESI†).

To gain further insight into the differences in device performance, photothermal deflection spectroscopy (PDS) was carried out (Fig. S23, ESI†). The Urbach energy U_E which can be extracted from the PDS measurements is related to energetic disorder in the material. **P10** with the highest mobility exhibits a lower Urbach energy and slightly less sub-band gap states than the alkylphenyl-substituted **P1** (U_E(**P10**) = 36 meV; U_E(**P1**) = 49 meV). This trend indicates larger energetic disorder of **P1** which is in agreement with its lower mobility.

GIWAXS measurements

The impact of the side chain architecture on morphology was analysed by grazing incidence wide angle X-ray scattering (GIWAXS) measurements. The films were prepared using the same conditions as for OFETs. The results are represented in Fig. 6.

Table 3 OFET characteristics of selected PIDTBT copolymers

Entry	R^1	R^2/R^3	On/off ratio	μ_{sat}/cm^2 V^{-1} s^{-1}
P1	Ph_6		$\sim 10^5$	3.5×10^{-2}
P3	Ph_6		$\sim 10^5$	4.0×10^{-2}
P5	Ph_8		$\sim 10^6$	3.8×10^{-2}
P8	Ph_8		$\sim 10^6$	3.9×10^{-2}
P9	Ph_8		$\sim 10^5$	2.2×10^{-2}
P10	$C_{12}H_{25}$		$\sim 10^6$	3×10^{-1}
P11		Me/Ph_{20}	$\sim 10^1$	1×10^{-4}
P12		Me/Ph_{20}	$\sim 10^2$	1.2×10^{-6}
P13		Ph_{20}/Ph_{20}	$\sim 10^1$	7.4×10^{-5}

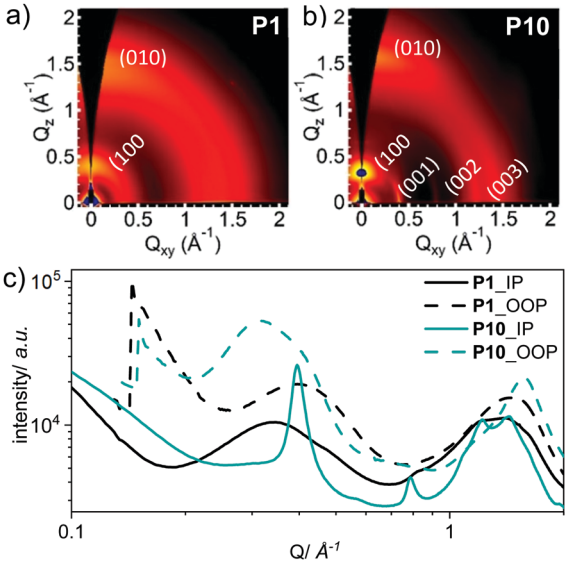

Fig. 6 2D GIWAXS images of **P1** (a) and **P10** (b) polymer films and comparison of in-plane (IP) and out-of-plane (OOP) diffraction patterns (c).

The alkylphenyl-substituted PIDTBT **P1** film shows broader peaks compared to the alkyl-substituted **P10** indicating a less ordered stacking and is in agreement with the previous observations from optical, thermal and charge transport characterization. The GIWAXS pattern of **P10** is consistent with previous measurements of alkyl-substituted PIDTBT,[1,3] with a prominent (010) (π-stacking) peak located in the out-of-plane direction Q_Z = 1.57 Å^{-1} corresponding to a π–π stacking of 4.0 Å. There are also a series of sharp in-plane reflections observed for **P10** which are indexed to backbone reflections with the (001) peak appearing at Q_{XY} = 0.395 Å^{-1} corresponding to a *d*-spacing of 15.9 Å. There is also a diffuse peak at $Q_Z \sim 0.3$ Å^{-1} in the out-of-plane direction. The indexing of this peak is uncertain; it is reminiscent of a lamellar stacking peak, but its appearance along Q_Z is inconsistent with the otherwise face-on texture of **P10**. This peak could be associated with a disordered, edge-on population[3] or reflect a more complicated unit cell. In contrast to **P10**, **P1** shows an absence of backbone reflections, with a broader (010) peak. The broad ring at Q = 1.4 Å^{-1} – which is reflective of amorphous chains – is also more prominent in **P1** compared to **P10**. Overall, the scattering data indicating increased order for **P10** with aliphatic side chains is in full accordance with DSC, UV-vis spectroscopy and PDS, and provides an explanation for the observed charge transport behaviour in this series of polymers.

Conclusions

We have presented two synthetic pathways towards PIDTBT copolymers using direct arylation for all C–C coupling steps. **Route A** relies on a classical DAP approach in which preformed monomers undergo polycondensation to give well-defined PIDTBT. **Route B** proceeds *via* a polyketone precursor also made *via* DAP following polymer analogous cyclization.

The comprehensive investigation of PIDTBT prepared by these different routes, with different molecular weights as well as different side chains revealed that (i) **route A** is superior compared to **route B** in terms of structural defects, (ii) optical properties of PIDTBT made *via* **route A** are strongly influenced by molecular weight, (iii) PIDTBT with alkylphenyl side chains exhibits MW-independent field-effect hole mobilities in the range of 10^{-2} cm^2 V^{-1} s^{-1} due to a mostly amorphous structure and (iv) PIDTBT with aliphatic C12 side chains and made *via* **route A** shows increased order, lower energetic disorder and accordingly higher field-effect hole mobilities on the order of 10^{-1} cm^2 V^{-1} s^{-1}. Thus, the presence or absence of phenyl rings in the side chains of PIDTBT has drastic consequences for packing, which is relevant for both transistor performance[3,16,47] as well as stability of blends with IDT-based components used for non-fullerene solar cells.[48]

Regarding a more comprehensive analysis of defects in PIDTBT made *via* **route B**, and neither proven nor unproven homocouplings in PIDTBT made *via* **route A**, further model compounds as well as significantly extended spectroscopic investigations will be required to make finale statements. A full homocoupling analysis of PIDTBT is generally much more challenging compared to other copolymers due to broad signals in ^{1}H NMR spectra. Unless irregularities between different samples show up, such study does not appear rewarding, and there is also no reason to assume their presence at this point.

Experimental

Instrumentation and methods

Detailed information about instrumentation, experimental procedures and theoretical calculations are described in the ESI.†

Materials

All starting materials were purchased from commercial sources and used without further purification unless otherwise specified. All reactions were carried out in flame dried glassware and under dry inert gas atmosphere. Compounds Ph_xIDT, K and TBT were synthesized according to published protocols.[17,33,49] Detailed ^{1}H and ^{13}C NMR analyses of the precursor polymer **P(K-*alt*-TBT)** are reported in the ESI† (Fig. S8 and S9).

Synthetic procedures

Representative procedure for synthesis of PIDTBT *via* DAP (P8). Ph_8IDT (54.2 mg, 53 μmol, 1 eq.), 4,7-dibromo-2,1,3-benzothiadiazole (15.6 mg, 53 μmol, 1 eq.), pivalic acid (5.3 mg, 53 μmol, 1 eq.) and potassium carbonate (22.0 mg, 158 μmol, 3 eq.) were placed in a vial and dissolved in 0.53 mL degassed mesitylene. Then Pd_2dba_3 (2.4 mg, 5 mol%) and P(*o*-anisyl)$_3$ (3.8 mg, 20 mol%) were added under argon and stirred for 72 h at 100 °C. After cooling to room temperature, the mixture was diluted with chloroform, precipitated into methanol and purified by Soxhlet extraction with acetone, ethyl acetate and chloroform. The chloroform fraction was filtered through a silica gel plug and dried overnight in a vacuum oven at 50 °C to afford a dark blue solid. Yield: 58.4 mg (95%).

Synthesis of P(K-*alt*-TBT). Compound K (738 mg, 0.74 mmol, 1 eq.), 4,7-di(thiophene-2-yl)-2,1,3-benzothiadiazole (221 mg, 0.74 mmol, 1 eq.), pivalic acid (75.2 mg, 0.74 mmol, 1 eq.) and potassium carbonate (305 mg, 2.21 mmol, 3 eq.) were placed in a vial and dissolved in 2.9 mL degassed mesitylene. Then Pd_2dba_3 (33.7 mg, 5 mol%) and P(*o*-anisyl)$_3$ (51.9 mg, 20 mol%) were added under argon and the whole was stirred for 72 h at 90 °C. Then 4.5 mL degassed bromobenzene was added under argon and stirred for another 24 h at 90 °C. After cooling to room temperature, the mixture was diluted with chloroform, precipitated into methanol and purified by Soxhlet extraction with acetone, ethyl acetate and chloroform. The chloroform fraction was filtered through a silica gel plug to afford a red solid. Yield: 638 mg (75%).

General procedure to Me/Ph_{20}-PIDTBT (P11, P12) and Ph_{20}/Ph_{20}-PIDTBT (P13). To a solution of **P(K-*alt*-TBT)** (200 mg, 0.17 mmol, 1 eq.) in 40 mL toluene at room temperature the corresponding lithium compound (1.40 mmol, 8 eq.) was added and after 30 minutes 5 mL THF was added. After stirring for 3 h at room temperature, the reaction mixture was quenched with ethanol and water, extracted with chloroform and dried over magnesium sulfate. The solvent was removed under vacuum and the crude product was immediately dissolved in dry chloroform. After the addition of boron trifluoride diethyl etherate (0.42 mL, 471 mg, 3.22 mmol, 18 eq.) the mixture was stirred for 3 h at room temperature and then quenched with ethanol and water, extracted with chloroform and dried over magnesium sulfate. The crude product was precipitated into methanol and purified by Soxhlet extraction with acetone, ethyl acetate and chloroform. The chloroform fraction was filtered through a silica gel plug to afford the title compounds as dark blue solid.

Me/Ph_{20}-PIDTBT. Yield: 10 mg (5%).

Ph_{20}/Ph_{20}-PIDTBT. Yield: 233 mg (73%).

Conflicts of interest

There are no conflicts to declare.

Acknowledgements

The authors thank M. Raisch for initial DSC measurements and D. Stegerer for TGA measurements. M. S. thanks the DFG (project SO 1213/8-2) for funding. A. P., A. S., B. P. and M. C. acknowledge funding from the European Research Council (ERC) under the European Union's Horizon 2020 research and innovation programme "HEROIC", Grant Agreement 638059. This work has been partially carried out at Polifab, the micro- and nanotechnology center of the Politecnico di Milano. S. H. and C. M. acknowledge funding from the Knut and Alice Wallenberg Foundation through the project "Mastering Morphology for Solution-borne Electronics". This work was performed in part at the SAXS/WAXS beamline[50] at the Australian

Synchrotron, part of ANSTO. We thank Jaime Martín for insightful discussions. F. O. would like to thank the DFG for funding through projects OR 349/1 and OR 349/3 and the Zentrum für Informationsdienste und Hochleistungsrechnen of TU Dresden for grants of computing time.

Notes and references

1 W. Zhang, J. Smith, S. E. Watkins, R. Gysel, M. McGehee, A. Salleo, J. Kirkpatrick, S. Ashraf, T. Anthopoulos, M. Heeney and I. McCulloch, *J. Am. Chem. Soc.*, 2010, **132**, 11437–11439.

2 H. Bronstein, D. S. Leem, R. Hamilton, P. Woebkenberg, S. King, W. Zhang, R. S. Ashraf, M. Heeney, T. D. Anthopoulos, J. de Mello and I. McCulloch, *Macromolecules*, 2011, **44**, 6649–6652.

3 X. Zhang, H. Bronstein, A. J. Kronemeijer, J. Smith, Y. Kim, R. J. Kline, L. J. Richter, T. D. Anthopoulos, H. Sirringhaus, K. Song, M. Heeney, W. Zhang, I. McCulloch and D. M. DeLongchamp, *Nat. Commun.*, 2013, **4**, 2238.

4 R. S. Ashraf, B. C. Schroeder, H. A. Bronstein, Z. Huang, S. Thomas, R. J. Kline, C. J. Brabec, P. Rannou, T. D. Anthopoulos, J. R. Durrant and I. McCulloch, *Adv. Mater.*, 2013, **25**, 2029–2034.

5 D. Venkateshvaran, M. Nikolka, A. Sadhanala, V. Lemaur, M. Zelazny, M. Kepa, M. Hurhangee, A. J. Kronemeijer, V. Pecunia, I. Nasrallah, I. Romanov, K. Broch, I. McCulloch, D. Emin, Y. Olivier, J. Cornil, D. Beljonne and H. Sirringhaus, *Nature*, 2014, **515**, 384–388.

6 I. McCulloch, R. S. Ashraf, L. Biniek, H. Bronstein, C. Combe, J. E. Donaghey, D. I. James, C. B. Nielsen, B. C. Schroeder and W. Zhang, *Acc. Chem. Res.*, 2012, **45**, 714–722.

7 Y. Li, M. Gu, Z. Pan, B. Zhang, X. Yang, J. Gu and Y. Chen, *J. Mater. Chem. A*, 2017, **5**, 10798–10814.

8 C. Liang and H. Wang, *Org. Electron.*, 2017, **50**, 443–457.

9 C.-P. Chen, S.-H. Chan, T.-C. Chao, C. Ting and B.-T. Ko, *J. Am. Chem. Soc.*, 2008, **130**, 12828–12833.

10 K.-S. Chen, Y. Zhang, H.-L. Yip, Y. Sun, J. A. Davies, C. Ting, C.-P. Chen and A. K.-Y. Jen, *Org. Electron.*, 2011, **12**, 794–801.

11 A. Wadsworth, M. Moser, A. Marks, M. S. Little, N. Gasparini, C. J. Brabec, D. Baran and I. McCulloch, *Chem. Soc. Rev.*, 2019, **48**, 1596–1625.

12 G. Zhang, J. Zhao, P. C. Y. Chow, K. Jiang, J. Zhang, Z. Zhu, J. Zhang, F. Huang and H. Yan, *Chem. Rev.*, 2018, **118**, 3447–3507.

13 C. Yan, S. Barlow, Z. Wang, H. Yan, A. K.-Y. Jen, S. R. Marder and X. Zhan, *Nat. Rev. Mater.*, 2018, **3**, 18003.

14 M. Nikolka, K. Broch, J. Armitage, D. Hanifi, P. J. Nowack, D. Venkateshvaran, A. Sadhanala, J. Saska, M. Mascal, S.-H. Jung, J. Lee, I. McCulloch, A. Salleo and H. Sirringhaus, *Nat. Commun.*, 2019, **10**, 2122.

15 Z. A. Lamport, K. J. Barth, H. Lee, E. Gann, S. Engmann, H. Chen, M. Guthold, I. McCulloch, J. E. Anthony, L. J. Richter, D. M. DeLongchamp and O. D. Jurchescu, *Nat. Commun.*, 2018, **9**, 5130.

16 A. Wadsworth, H. Chen, K. J. Thorley, C. Cendra, M. Nikolka, H. Bristow, M. Moser, A. Salleo, T. D. Anthopoulos, H. Sirringhaus and I. McCulloch, *J. Am. Chem. Soc.*, 2020, **142**, 652–664.

17 W. Gao, M. Zhang, T. Liu, R. Ming, Q. An, K. Wu, D. Xie, Z. Luo, C. Zhong, F. Liu, F. Zhang, H. Yan and C. Yang, *Adv. Mater.*, 2018, **30**, 1800052.

18 T. W. Bünnagel, B. S. Nehls, F. Galbrecht, K. Schottler, C. J. Kudla, M. Volk, J. Pina, J. S. S. de Melo, H. D. Burrows and U. SCherf, *J. Polym. Sci., Part A: Polym. Chem.*, 2008, **46**, 7342–7353.

19 Y. Ma, Q. Zheng, Z. Yin, D. Cai, S.-C. Chen and C. Tang, *Macromolecules*, 2013, **46**, 4813–4821.

20 Y.-C. Chen, C.-Y. Yu, Y.-L. Fan, L.-I. Hung, C.-P. Chen and C. Ting, *Chem. Commun.*, 2010, **46**, 6503.

21 A. S. Dudnik, T. J. Aldrich, N. D. Eastham, R. P. H. Chang, A. Facchetti and T. J. Marks, *J. Am. Chem. Soc.*, 2016, **138**, 15699–15709.

22 S. Holliday, Y. Li and C. K. Luscombe, *Prog. Polym. Sci.*, 2017, **70**, 34–51.

23 P.-O. Morin, T. Bura and M. Leclerc, *Mater. Horiz.*, 2016, **3**, 11–20.

24 R. Matsidik, H. Komber, A. Luzio, M. Caironi and M. Sommer, *J. Am. Chem. Soc.*, 2015, **137**, 6705–6711.

25 R. Matsidik, H. Komber and M. Sommer, *ACS Macro Lett.*, 2015, **4**, 1346–1350.

26 F. Nübling, H. Komber and M. Sommer, *Macromolecules*, 2017, **50**, 1909–1918.

27 A. E. Rudenko and B. C. Thompson, *J. Polym. Sci., Part A: Polym. Chem.*, 2015, **53**, 135–147.

28 M. Wakioka and F. Ozawa, *Asian J. Org. Chem.*, 2018, **7**, 1206–1216.

29 J.-R. Pouliot, F. Grenier, J. T. Blaskovits, S. Beaupré and M. Leclerc, *Chem. Rev.*, 2016, **116**, 14225–14274.

30 S. Chen, K. C. Lee, Z.-G. Zhang, D. S. Kim, Y. Li and C. Yang, *Macromolecules*, 2016, **49**, 527–536.

31 Y. Li, W. K. Tatum, J. W. Onorato, S. D. Barajas, Y. Y. Yang and C. K. Luscombe, *Polym. Chem.*, 2017, **8**, 5185–5193.

32 Y. Li, W. K. Tatum, J. W. Onorato, Y. Zhang and C. K. Luscombe, *Macromolecules*, 2018, **51**, 6352–6358.

33 D. Adamczak, H. Komber, A. Illy, A. D. Scaccabarozzi, M. Caironi and M. Sommer, *Macromolecules*, 2019, **52**, 7251–7259.

34 Y. Yao and J. M. Tour, *Macromolecules*, 1999, **32**, 2455–2461.

35 F. Lombeck, H. Komber, S. I. Gorelsky and M. Sommer, *ACS Macro Lett.*, 2014, **3**, 819–823.

36 M. S. Vezie, S. Few, I. Meager, G. Pieridou, B. Dörling, R. S. Ashraf, A. R. Goñi, H. Bronstein, I. McCulloch, S. C. Hayes, M. Campoy-Quiles and J. Nelson, *Nat. Mater.*, 2016, **15**, 746–753.

37 M. J. Frisch, *et al.*, *Gaussian 16 Rev. C.01*, Wallingford, CT, 2016.

38 K. S. Schellhammer, T.-Y. Li, O. Zeika, C. Körner, K. Leo, F. Ortmann and G. Cuniberti, *Chem. Mater.*, 2017, **29**, 5525–5536.

39 S. Chibani, B. Le Guennic, A. Charaf-Eddin, O. Maury, C. Andraud and D. Jacquemin, *J. Chem. Theory Comput.*, 2012, **8**, 3303–3313.

40 C. Müller, *Chem. Mater.*, 2015, **27**, 2740–2754.
41 M. Xiao, A. Sadhanala, M. Abdi-Jalebi, T. H. Thomas, X. Ren, T. Zhang, H. Chen, R. L. Carey, Q. Wang, S. P. Senanayak, C. Jellett, A. Onwubiko, M. Moser, H. Liao, W. Yue, I. McCulloch, M. Nikolka and H. Sirringhaus, *Adv. Funct. Mater.*, 2020, 2007359.
42 J. Martín, N. Stingelin and D. Cangialosi, *J. Phys. Chem. Lett.*, 2018, **9**, 990–995.
43 L. Yu, D. Qian, S. Marina, F. A. A. Nugroho, A. Sharma, S. Hultmark, A. I. Hofmann, R. Kroon, J. Benduhn, D.-M. Smilgies, K. Vandewal, M. R. Andersson, C. Langhammer, J. Martín, F. Gao and C. Müller, *ACS Appl. Mater. Interfaces*, 2019, **11**, 21766–21774.
44 R. Xie, A. R. Weisen, Y. Lee, M. A. Aplan, A. M. Fenton, A. E. Masucci, F. Kempe, M. Sommer, C. W. Pester, R. H. Colby and E. D. Gomez, *Nat. Commun.*, 2020, **11**, 893.
45 F. Kempe, F. Riehle, H. Komber, R. Matsidik, M. Walter and M. Sommer, *Polym. Chem.*, 2020, **11**, 6928–6934.
46 L. Wang, D. Fine, D. Basu and A. Dodabalapur, *J. Appl. Phys.*, 2007, **101**, 054515.
47 M. Nikolka, M. Hurhangee, A. Sadhanala, H. Chen, I. McCulloch and H. Sirringhaus, *Adv. Electron. Mater.*, 2018, **4**, 1700410.
48 S. Hultmark, S. H. K. Paleti, A. Harillo, S. Marina, F. A. A. Nugroho, Y. Liu, L. K. E. Ericsson, R. Li, J. Martín, J. Bergqvist, C. Langhammer, F. Zhang, L. Yu, M. Campoy-Quiles, E. Moons, D. Baran and C. Müller, *Adv. Funct. Mater.*, 2020, **30**, 2005462.
49 F. Lombeck, H. Komber, A. Sepe, R. H. Friend and M. Sommer, *Macromolecules*, 2015, **48**, 7851–7860.
50 N. M. Kirby, S. T. Mudie, A. M. Hawley, D. J. Cookson, H. D. T. Mertens, N. Cowieson and V. Samardzic-Boban, *J. Appl. Crystallogr.*, 2013, **46**, 1670–1680.